An Analytical Model for Predicting the Effective Thermal Conductivity of Woven Wire Wick Structure

Jin Sung Lee* and Chul Ju Kim**

Key words: Woven wire wick, Porosity, Effective thermal conductivity

Abstract

Woven wire wick is a very effective structure because of its easiness to insert inside of pipe for a miniature heat pipe. The present study was conducted to predict the porosity and the effective thermal conductivity of liquid-saturated woven wire wick. The porosity and the effective thermal conductivity of the evaporator region indicate different values from those of the condenser region due to the existence of non-flow region. The minimum value of the effective thermal conductivity indicates on condition of the $\theta=45°$ and the values of the effective thermal conductivity increases symmetrically centering around the minimum value. The values of the effective thermal conductivity in the evaporator region at the angle of 45° indicate about 60~80% higher than those in the condenser region for various combinations of copper, and stainless with water and ethanol.

Nomenclature

a : length of liquid flow region normal to wire length
a' : length defined by Eq. (8)
A : area
A_w : cross sectional area of wire
b : length of non-flow region normal to wire length
b' : length defined by Eq. (8)
c : length of interval between two wires
d : thickness of wire
D_i : inner diameter of tube
k : thermal conductivity
n : numbers of wire for a wire group
N : numbers of wire group
L_o : length of wire for a 1 turn
R : thermal resistance
T_s : saturation temperature
V : volume
X : length, $a+b$

Greek symbols

α : angle, $|2\theta-(\pi/2)|$

* Computational Science & Engineering (CSE) Center, Samsung Advanced Institute of Technology P.O. Box 111, Suwon 440-600, Korea
** School of Mechanical Engineering, Sungkyunkwan University, 300 Chunchun-dong, Suwon 440-746, Korea

ε : porosity
θ : wire helix angle

Subscripts

con : condenser
eff : effective
eva : evaporator
f : fluid
s : solid
t : total

1. Introduction

Heat pipes have been successfully used in various applications such as thermal control, heat exchangers and electronic cooling. Especially, miniature heat pipes have been attracted lately due to their many advantages, such as geometry adaption, ability for localized heat dissipation and the production of an uniform temperature fields.

So far, many investigations have been reported on the performance of miniature heat pipe.[1 5] Generally, the groove and screen wick have been used for a small heat pipe as a wick structure. The heat transfer limitation of the groove wick shows very low values in comparison with the other wick structure due to the weak capillary force.[6 8] The screen wick is the most commonly used wick structure, but it has a difficulty to change the shape and to insert inside a small size pipe. In the present study, an analytic approach has been employed to predict the porosity and the effective thermal conductivity for a woven wire wick structure. Figure 1 shows woven wire wick structure. The woven wire wick structure is formed by the several wire groups (N=4~8), and each group is composed of numbers of wire (n=4~8). The woven wire wick is a very effective structure because of its availability and easiness to insert inside of the pipe. The effective thermal conductivity of the wick is dependent on both the solid wick and the working fluid. Under normal heat pipe operation, a major portion of heat is transferred across a liquid-vapor interface in the evaporator and condenser regions. So, It is important to determine the effective thermal conductivity of the wick for designing the heat pipe. The porosity and the effective thermal conductivity of a woven wire wick are different significantly in the evaporator and condenser region due to the existence of the non-flow region. In the condenser region, vapor is condensed over the entire surface, as shown in Fig. 1. This includes the liquid-vapor interface over both the liquid flow passage and the non-flow region. However, in the evaporator region, most of the liquid is evaporated at the liquid flow passage.

Fig. 1 Woven wire wick structure.

The present study represents an attempt to explore analytically the porosity and the effective thermal conductivity for a woven wire wick structure. Also, this study demonstrates that the porosity and the effective thermal conductivity values are obtained differently in the evaporator and condenser regions.

2. Analytical model

Figure 2 shows the plain view of a woven wire wick structure for one turn. The cross section $y-y'$ indicates the liquid flow passage section (a) and the non-flow region (b). The liquid flow passage a is

$$a = nd + (n-1)c \tag{1}$$

where c, d are the length of interval between

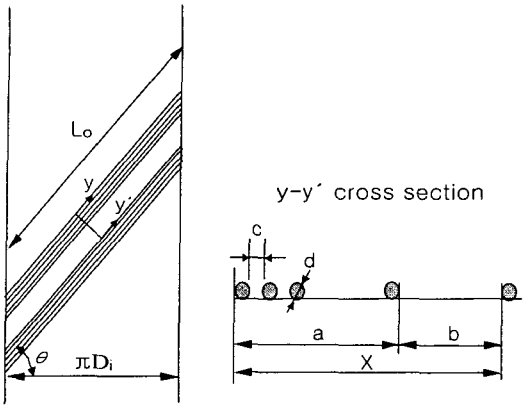

Fig. 2 A plain view of woven wire wick structure for one turn.

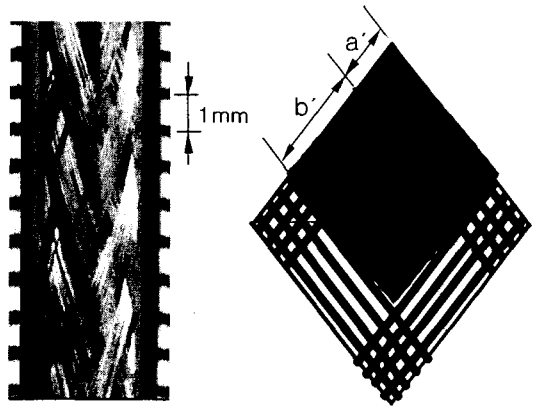

Fig. 3 Weaving pattern and unit cell model of a woven wire wick.

wires and the thickness of the wire, respectively. n is the numbers of wire for a wire group. The wire length for one turn is L_o and the wire inclination angle is θ, we can express a relationship as follows

$$L_o \cos\theta = \pi D_i \tag{2}$$

The inner circumferential length of the tube can be expressed by the following equation

$$\pi D_i \sin\theta = (a+b)N \tag{3}$$

where N is the numbers of wire group. Rearranging equations (2) and (3)

$$X = \frac{L_o \sin\theta \cos\theta}{N} \tag{4}$$

where $X = a+b$.

Figure 3 shows the weaving pattern and a unit cell model employed in this study. With this geometric model, the unit cell can be rearranged into four sections. The section 1 is for the two crossed wire groups, section 2, 3 is for the single wire group, and section 4 is for fluid only. A quarter section of the region could be used in the analysis due to symmetry, but the whole section is considered for clarity. The area of each section can be expressed are

$$A_1 = \frac{a^2}{4\cos\alpha} \tag{5}$$

$$A_2 = A_3 = \frac{ab}{2\cos\alpha} \tag{6}$$

$$A_4 = \frac{b^2}{\cos\alpha} \tag{7}$$

$$a = 2a'\cos\alpha, \quad b = b'\cos\alpha \tag{8}$$

where, $\alpha = \left|2\theta - \frac{\pi}{2}\right|$.

The total volume of each region can be expressed are

$$V_1 = 8A_1 d \tag{9}$$

$$V_2 = 2A_2 d \tag{10}$$

$$V_3 = 3A_2 d \tag{11}$$

$$V_4 = 1.25A_3 d \tag{12}$$

In Eqs. (11) and (12), the volumes of V_3 and V_4 are expressed based on the equivalent depth using the mean values of each section. The equivalent depths of V_3 and V_4 are $1.5\,d$ and $1.25\,d$, respectively. The volume of fluid flow passage at each region can be expressed as follows

$$V_{f,1} = 8(A_1 d - a' A_w n) \tag{13}$$

$$V_{f,2} = 2(A_2 d - b' A_w n) \tag{14}$$

$$V_{f,3} = 2(A_2 1.5d - b' A_w n) \tag{15}$$

$$V_{f,4} = 1.25 A_3 d \tag{16}$$

where, $A_w = \frac{\pi}{4} d^2$.

The porosity of each section are expressed by the ratio of fluid passage to total volume.

$$\varepsilon_i = \frac{V_{f,i}}{V_i} \quad (i=1,2,3) \tag{17}$$

The mean porosity of the evaporator and condenser regions are the summation value of each section.

$$\bar{\varepsilon}_{eva} = \frac{\sum_{i=1}^{3} V_{f,i}}{\sum_{i=1}^{3} V_i} \tag{18}$$

$$\bar{\varepsilon}_{con} = \frac{\sum_{i=1}^{4} V_{f,i}}{\sum_{i=1}^{4} V_i} \tag{19}$$

In Eqs. (18) and (19), the mean porosity indicate different values in the evaporator and the condenser regions. This is due to the fact of the existence of the non-flow region. In the condenser region, vapor is condensed over the entire surface. This includes the liquid-vapor interface over both the liquid flow passage and the non-flow region. However, in the evaporator region, most of the liquid is evaporated at the liquid flow passage.

Thermal resistance in series through each section may be written as

$$R_1 = \frac{\varepsilon_1 2d}{k_f A_1} + \frac{(1-\varepsilon_1)2d}{k_s A_1} \tag{20}$$

$$R_2 = \frac{\varepsilon_2 d}{k_f A_2} + \frac{(1-\varepsilon_2)d}{k_s A_2} \tag{21}$$

$$R_3 = \frac{\varepsilon_3 1.5d}{k_f A_2} + \frac{(1-\varepsilon_3)1.5d}{k_s A_2} \tag{22}$$

$$R_4 = \frac{1.25d}{k_f A_3} \tag{23}$$

From the parallel thermal circuit

$$\frac{1.625d}{k_{eff,eva} A_{t,eva}} = \frac{4}{R_1} + \frac{2}{R_2} + \frac{2}{R_3} \tag{24}$$

$$\frac{1.58d}{k_{eff,con} A_{t,con}} = \frac{4}{R_1} + \frac{2}{R_2} + \frac{2}{R_3} + \frac{1}{R_4} \tag{25}$$

In Eqs. (24) and (25), $1.625d$ and $1.58d$ are used as a equivalent depth based on the mean values of the evaporator and the condenser regions, respectively. Rearranging yields

$$k_{eff,eva} = \frac{0.813 R_1 R_2 R_3 d}{A_{t,eva}(R_1 R_2 + R_1 R_3 + 2R_2 R_3)} \tag{26}$$

$$k_{eff,con} = \frac{1.58 R_1 R_2 R_3 R_4 d}{A_{t,con}[R_1 R_2 (R_3 + 2R_4) + R_3 R_4 (2R_1 + 4R_2)]} \tag{27}$$

where, $A_{t,eva} = \sum_{i=1}^{3} A_i$, $A_{t,con} = \sum_{i=1}^{4} A_i$

3. Results and discussion

Figure 4 shows the values of the length X

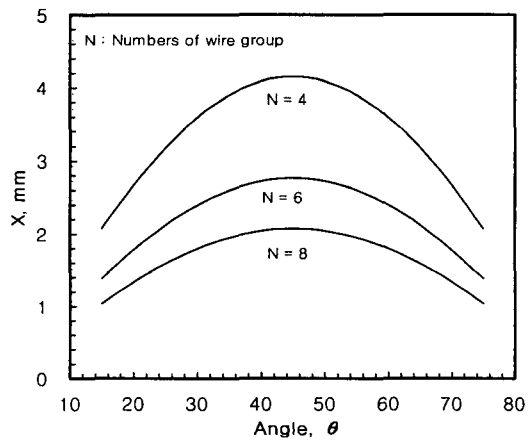

Fig. 4 Variations of length X as a function of wire helix angle for several values of N.

versus wire helix angle for various values of N. More that the values of X, obtained from Eq. (4), means the summation length of the liquid flow passage and the non-flow region perpendicular to the wire direction, and L_o means the length of wire for one turn. According to the experimental measurements for various tube inner diameters inserted to the woven wire wick, the values of L_o are about 33.2 mm in the range of tube diameter $3 \leq D_i \leq 7$. It can be seen in Fig. 4 that as the number of N decreases, the length X tends to be long, and reveals a maximum value under the condition of $\theta = 45°$.

Figure 5 shows the variation of area $A_1 \sim A_4$, obtained from Eqs. (5)~(7), are plotted as a function of wire helix angle. In Fig. 5, the values of each c and d and n and N are 0.06 mm and 8, respectively. Because the area A_4 is the non-flow region, heat transfer does not occur in the evaporator region. However, in the condenser region, the vapor condenses all of the region $A_1 \sim A_4$. Thus, it is essential considering the effective heat transfer area when the design miniature heat pipe is inserted into the woven wire wick. As shown in Fig. 5, the non-flow region A_4 varies largely dependent on the wire helix angle in comparison with the variation of the flow passage region $A_1 \sim A_3$. At the wire helix angle of 45°, the area of non-flow region A_4 almost equals the summation of the liquid flow passage region $A_1 \sim A_3$.

Figure 6 shows the variations of the mean porosity as a function of wire helix angle under various numbers of N. The mean porosity of the evaporator and condenser regions are calculated from Eqs. (18) and (19) on the condition of c, d=0.06 mm and n=8. In the evaporator region, the mean porosity variations with respect to the wire helix angle and the number of N tend to be small, because the volume of liquid flow passage varies very slightly. On the other hand, in the condenser region, the mean porosity varies largely dependent on the wire helix angle and the number of N because the volume of the non-flow region varies to a great extent. The maximum mean porosity occurs on the condition of θ=45° and the values of porosity decreases monotonically from the maximum value. In the case of N=8, the value of the mean porosity in the condenser region

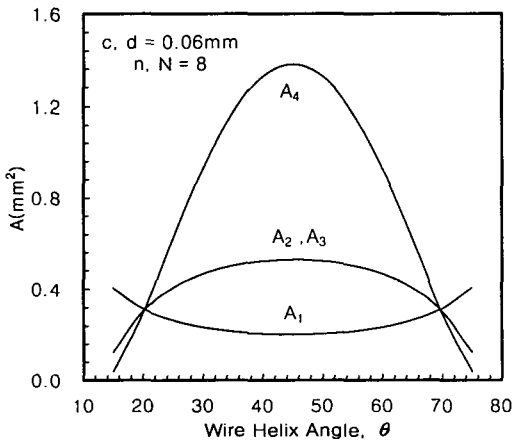

Fig. 5 Variations of areas as a function of wire helix angle.

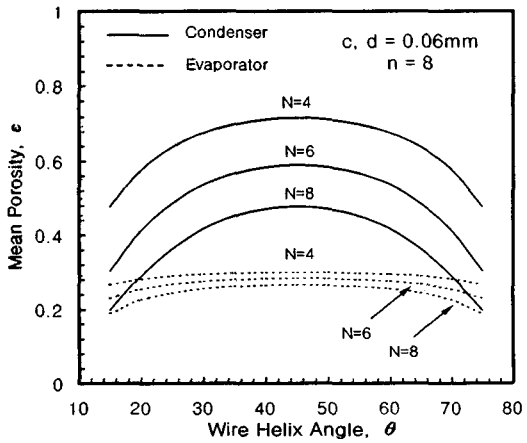

Fig. 6 Variations of mean porosity as a function of wire helix angle for several values of N.

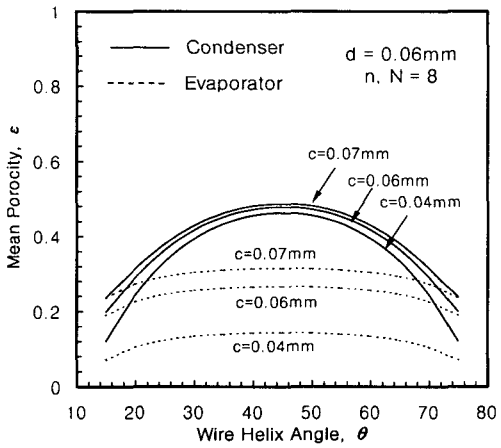

Fig. 7 Variations of mean porosity as a function of wire helix angle for several values of c.

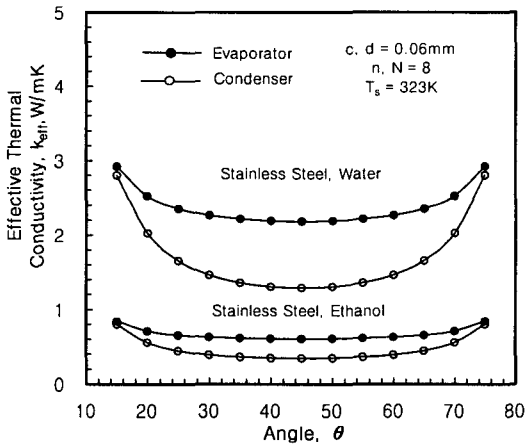

Fig. 9 Variations of effective thermal conductivity as a function of wire helix angle for Stainless steel wire saturated water and ethanol.

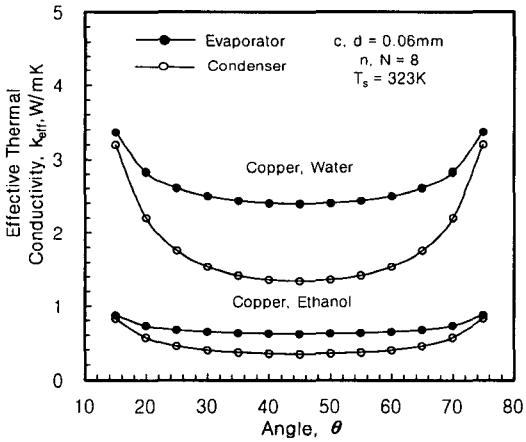

Fig. 8 Variations of effective thermal conductivity as a function of wire helix angle for copper wire saturated water and ethanol.

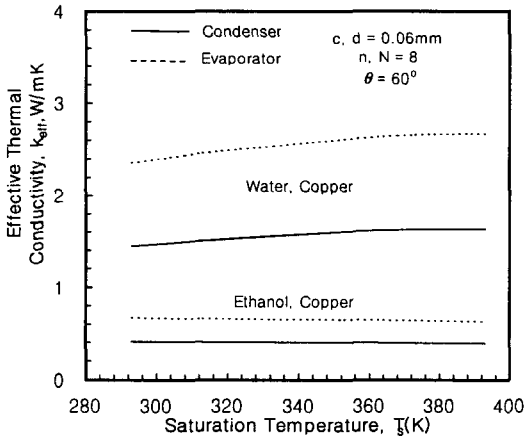

Fig. 10 Variations of effective thermal conductivity as a function of saturation temperature for copper wire saturated water and ethanol.

has about two times higher than that in the evaporator region.

Figure 7 shows the variations of the mean porosity as a function of the wire helix angle and the length of interval between wires. As the interval of wires changes in the range of c=0.04~0.07 mm, result in a variation of liquid flow passage, which consequently affect the mean porosity of the evaporator and the condenser region.

Figures 8 and 9 show the variations of the effective thermal conductivity as a function of wire helix angle for various combinations of solid wire materials and working fluids. Where the values of c, d and n, N are 0.06 mm and 8, respectively. The effective thermal conductivity is affected strongly by the wire helix angle due to the variations of the porosity.

The minimum value of effective thermal conductivity is obtained on the condition of $\theta=45°$ and the values of the thermal conductivity increases monotonically from the minimum value at $\theta=45°$. As in Figs. 8 and 9, the values of the effective thermal conductivity in the evaporator region at the angle of 45° have about 60~80% higher than those in the condenser region for various combinations of copper and stainless with water and ethanol. Figure 10 shows the variations of the effective thermal conductivity as a function of saturation temperature for various combinations of solid wire materials and working fluids. The variation of the effective thermal conductivity varies slightly in the range of saturation temperature of 300~400 K.

4. Conclusions

In the present study, an analytic approach has been employed to predict the porosity and the effective thermal conductivity for a woven wire wick structure. The porosity and the effective thermal conductivity of the evaporator region have different values from the values of the condenser region due to the existence of non-flow region. The minimum value of effective thermal conductivity is obtained on the condition of $\theta=45°$ and the effective thermal conductivity increases symmetrically from the minimum value. The effective thermal conductivity in the evaporator region at the angle of 45° has about 60~80% higher than that in the condenser region for various combinations of copper and stainless with water and ethanol. The present model requires more experimental data of the effective thermal conductivity and analytical research to generalize.

Reference

1. Noda, H. and Kumagai, M., 1999, Effect of mesh shape on maximum capillary pressure of plain weave screen, Proceedings of the 11th International Heat Pipe Conference, pp. 85-98.
2. Sauciuc, I., Mochizuki, M., Mashiko, K., Saito, Y. and Nguyen, T., 1999, The design and testing of an improved wick structure to be used in heat pipes for electronic cooling application, Proceedings of the 11th International Heat Pipe Conference, pp. 61-65.
3. Bazzo, E., Reimbrecht, E. G. and Fernandes, C. P., 1999, Manufacturing procedure and porous structure characterization of tubular wicks, Proceedings of the 11th International Heat Pipe Conference, pp. 264-268.
4. Akihiro, S., 1999, A flexible heat pipe with carbon fiber arterial wick, Proceedings of the 11th International Heat Pipe Conference, pp. 119-123.
5. Zuo, Z. J. and North, M. T., 1999, Improved heat pipe performance using graded wick structures, Proceedings of the 11th International Heat Pipe Conference, pp. 80-84.
6. Faghri, A., 1995, Heat Pipe Science and Technology, Taylor & Francis.
7. Chi, S. W., 1976, Heat Pipe Theory and Practice, Hemisphere Publishing Corporation.
8. Dunn, P. D. and Reay, D. A., 1994, Heat Pipes. Pergamon Press, 4th edition.